Journal of Ceramic Processing Research. Vol. 20, No. 2, pp. 187~197 (2019)

JOURNAL OF
Ceramic Processing Research

Effects of TiO_2 phases on the structural and dielectric properties of sintered $BaTiO_3$ + x% mol Fe_2O_3 ceramics

R. Bounouioua*, T. Bezzi, S.E. Berama, B. Boudine and M.T. Benlahrache
Ceramics laboratory-University of frères Mentouri of Constantine1, 25000, Algeria

The objective of this paper is to study the influence of TiO_2 phases on the structural and dielectric properties of the $BaTiO_3$ ceramics containing different amounts of Fe_2O_3. The pure $BaTiO_3$ ceramics was prepared by a solid state reaction between $BaCO_3$ and both of TiO_2 phases, anatase (A) and rutile (R), respectively. We prepared the mixtures by stoichiometric way, which were calcined at 1100 °C during 2hrs. The formations of perovskites structures ABO_3 were confirmed by X-rays diffraction analysis. While the ceramics mixture with (1-x) $BaTiO_3$+ x % Fe_2O_3 (where x = 1, 2, 5 and 7 wt %) compositions were prepared by the wet milling. Afterwards, the different pellets were fabricated by uniaxial compression and sintered at different temperatures (1300, 1350 and 1400 °C). The obtained results show an increase in the tetragonality due to the doping by Fe^{3+}, consequencely an increase in the relative permittivity of samples prepared from TiO_2(R) with both of Fe_2O_3 addition and sintering temperature. On the other hand, for the samples prepared from TiO_2 (A) the obtained results show a decrease in both relative density and tetragonality with both of Fe_2O_3 addition and sintering temperature, as a consequence we get a decrease in the relative permittivity compared with pure BTA.

Keys words: $BaTiO_3$ (A), $BaTiO_3$(R), TiO_2 phases, Tetragonal phase, Hexagonal phase, Dielectrics properties.

Introduction

The barium titanate ($BaTiO_3$) is a ferroelectric material with a perovskite structure prepared by solid state reaction between BaO and TiO_2, which acts as a catalyst for the decomposition of $BaCO_3$ to BaO [1], than $BaTiO_3$ formed by diffusion of Ba and O ions into the TiO_2 lattice [2], which is largely studied because of its electric properties, ferroelectricity, positive temperature coefficient of resistivity (PTCR), piezoelectricity,…etc. The electrical properties of based $BaTiO_3$ ceramics depend on different parameters such as powder impurity, particle morphology, particle size, grain boundary, additions [3].

Oxide additions are used to improve the dielectric properties of based $BaTiO_3$ ceramics. This is because the B-site Ti can be easily substituted by other transition metal ions. On the other hand, there are two types of oxides additions; acceptor type generally as trivalent cations M^{3+} when they substitute B-site such as Co^{3+}, Fe^{3+}, Bi^{3+}, Y^{3+}, Dy^{3+} [4-8], donor type as pentavalent cations M^{5+} such as Nb^{5+}, Ta^{5+}, P^{5+} when they substitute B- site[9]. When M^{3+} ions substitutes the A or B sites in the perovskite lattice ABO_3, the electrical conductivity showed an acceptor or donor doped behaviour depending on the A/B ratio [10]. A such behaviour can be explained by the following equation in Kröger-Vink notation:

Acceptor behaviour A/B>1: $M_2O_3 \rightarrow 2M'_B + 3O^X_O + V^{\cdot\cdot}_O$ (1)

donor behaviour A/B< 1: $M_2O_3 \rightarrow 2M^{\cdot}_A + 3O^X_O + 2e^-$ (2)

In the recent years, the phase transformation of Fe-doped $BaTiO_3$ ceramics were studied [6]. It was found that the B-site Ti can be substituted by Fe, at doping levels up to 10% (molar fraction). Both tetragonal and hexagonal phases coexisted in the Fe-doped $BaTiO_3$ ceramics [6], where the formation of hexagonal phase in the Fe-doped $BaTiO_3$ ceramics was promoted by higher doping levels of Fe, higher sintering temperature and longer sintering time.

The moment for addition metal ions (oxide addition) before or after calcination has a great effect on the results of conventional reaction. The addition after calcination favourites the formation of secondary phases and the addition before calcination favourites the formation of complex perovskite structure [11-13]. On the other hand, the ternary phase diagram of BaO-TiO_2-Fe_2O_3 was studied by Vanderah et al. [14], the authors put into evidence the presence of solid solution $Ba(Fe\text{-}Ti)O_{3\text{-}X}$ where x range is between 0.06 and 0.84 (molar fraction), and they concluded that iron substitution into the $BaTiO_3$ system stabilizes the hexagonal $BaTiO_3$ structure. Also Han-li et al [15] studied crystallite structure, microstructure, dielectric and ferroelectric properties of $BaTi_{0.99}Fe_{0.01}O_{3\text{-}d}$ ceramics, they found that Fe^{3+} ions were soluble into $BaTiO_3$ lattice with the given concentration (1% molar fraction) and a decrease in the

*Corresponding author:
Tel : +2137 76 17 85 85
Fax: +213 31 81 88 81
E-mail: Bounouiouarabah.phy@hotmail.com

tetragonality due to the doping of Fe^{3+}, in addition to the obtained ceramics has dense microstructure with decreased dielectric constant-Curie temperature and ferroelectric properties. Also, they found a diffuse phase transition on the dielectric constant-Curie temperature.Qiwei Lou et al. studied the Ferroelectric properties of Li^{+} doped $BaTiO_3$ ceramics [16]. They prepared the mixture by the solid state reaction method between commercial $BaTiO_3$ and Li_2CO_3, the obtained results show that the lattice structure, the grain size and the dielectric properties of Li-doped $BaTiO_3$ ceramics are dependent on Li site. They suggested that the role of oxygen vacancy accompanied by the Li-doping is important. In either hand, they conclude that Li^{+} prefers to favorably substitute Ba^{2+} at A site for the low amount of Li, but its location was changed to Ti^{4+} at B site for the large amount of Li.

The principal goal of this paper is to study the effects of TiO_2 phases on the $BaTiO_3$ perovskite structures and as consequently the effects of Fe^{3+} ion on the structural and dielectric properties of sintered $BaTiO_3$+x% mol. Fe_2O_3.

Experimental

$BaTiO_3$ (BT) powder used in this investigation was prepared in the laboratory following the conventional procedure of milling and calcinations. The starting raw materials used to prepare BT powder which have high purity commercial anatase phase TiO_2 (A) powder (Flukat, Japan) and local pure $BaCO_3$ (extracted out from Khroub locality in Algeria), rutile phase TiO_2(R) powder was prepared locally in the laboratory by calcinations of anatase phase TiO_2 in air at 1000 ºC for 10 hrs, and XRD analysis was carried out on calcined powders to control the formation of rutile phase, iron oxide Fe_2O_3 powder (Flukat, Japan). The starting powder were weighed and mixed in a stoichiometric proportion from $BaCO_3$ and both of the TiO_2 phases (A) and (R), respectively.

The mixtures were then ball-milled for 20 hrs using alumina balls in methanol alcohol. The obtained slurry was then dried at 80 ºC in electrical furnace and calcined in air at 1100 ºC for 2 hrs. The XRD analysis was carried out on calcined powders to control the formation of BT phase (both BT (A) and BT(R)). After that, (1-x) $BaTiO_3$ + x% mol. Fe_2O_3 (where x = 1, 2, 5 and 7) mixtures were prepared from BT (A), BT(R) and Fe_2O_3 powders and re-milled by the same route. Later, 13 mm in diameter and 5 mm in thickness of the pellets were fabricated by uniaxial cold press under 150 MPa. The pellets were, then, sintered in an electric furnace in air at, respectively, 1300 ºC, 1350 ºC and 1400 ºC for 2 hrs with a heating rate of 3 º/ min.

The obtained sintered samples were characterized in terms of apparent density by direct measure of mass and volume. The X-ray diffraction analysis (XRD, D8Advenced Bruker-Siemens Diffractometer, with Cu ka radiation) was carried out on different sintered samples to follow the microstructure evolution.

For dielectric characteristics, both surfaces of samples were metallised by Ag paste, then, they were heated in air at 700 ºC for 30 min. Then, the dielectric constant, dielectric loss and electrical resistivity as a function of temperature which were measured in the temperature rang (30-200 ºC) at 3 ºC/min by RLC meter (Philips type PM 6303) at 1 KHz .

Results and Discussion

The evolution of relative densities as function of iron oxides (Fe_2O_3) addition for samples prepared from both TiO_2 types sintered in air for 2hrs at different temperatures are shown in the Fig. 1. Here the obtained curves in Fig. 1(a) reveal identical evolution of the pellets relative density as function of sintering temperature for different % mol Fe_2O_3 used in this investigation; we see that there is an increase in relative

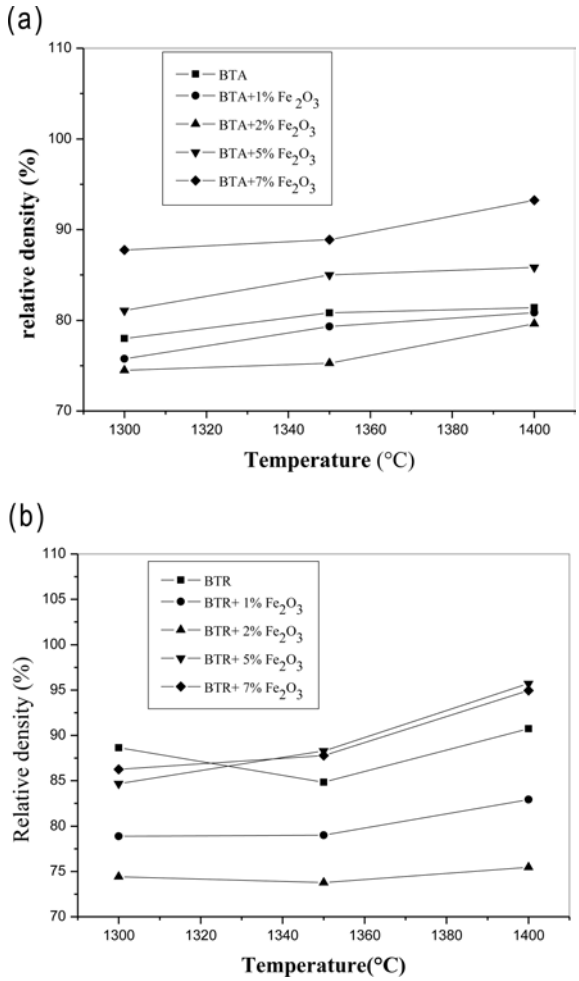

Fig. 1. Relative density of different pellets as function of sintering temperature.

density with an increasing in sintering temperature, also a decrease in relative density for 1% and 2% mol Fe_2O_3 additions with increasing sintering temperature compared with pure BTA.

Furthermore, we have an increase for 5% and 7% mol Fe_2O_3 additions. On the other hand, the high densification for all samples attain at sintering temperature at 1400 °C. In the Fig. 1(b), we show the decrease of relative density for the pure BTR, therefore, we have an increase with increasing in sintering temperature, and the same remark for different amounts of iron addition. Finally, it is clear that the pellets prepared from rutile phase have the higher densification compared with pellets prepared from anatase phase. Fig. 2(a) and 2(b) show the variation of the relative density as function of mol % Fe_2O_3 for different sintering temperatures. The minimum of the relative density was obtained in pellets containing 2 mol % of addition, then an increase appears for over-doped samples for different sintering temperature, on the other hand, the curves in Fig. 2(a) reveal two distinct domains for evolution of the relative density as function of mol.% Fe_2O_3, where the first domain range from 0 to 2, a manifest decrease in the pellets density is remarked for all considered temperature and the second domain range from 2 to 7, a manifest increase in the pellets density is remarked for all considered temperature. The same general observations were shown in the Fig.

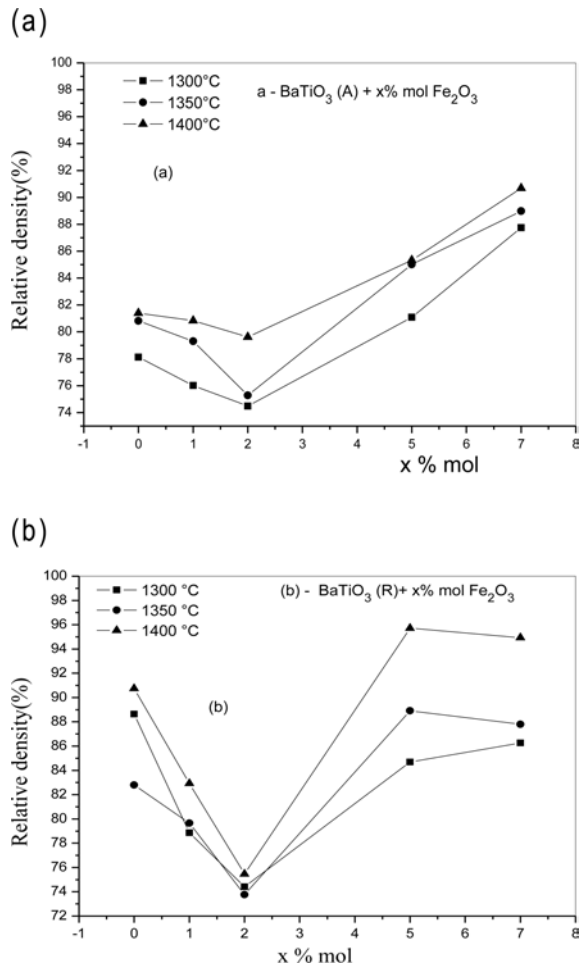

Fig. 2. Relative density of different pellets as function of Fe_2O_3 percentage (mol %).

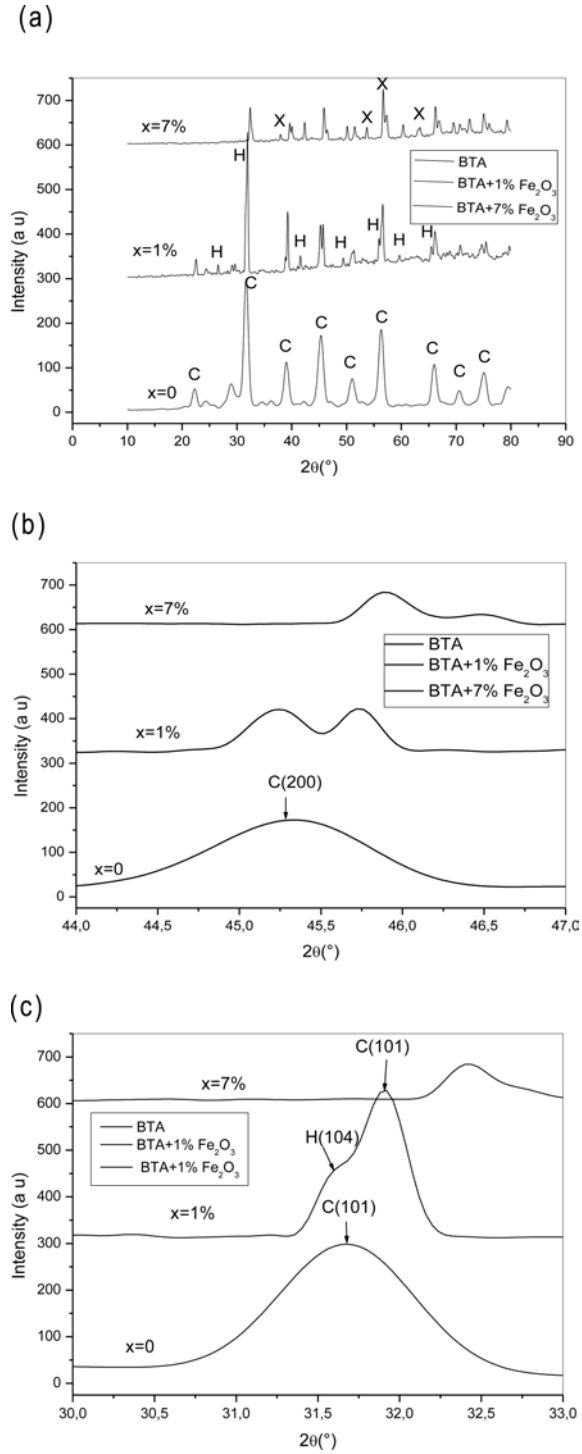

Fig. 3. a: XRD spectra recorded from BTA+ x % Fe_2O_3 samples sintered at 1400 °C for 2 hrs. C: Cubic, H: hexagonal, X: unknown phase. b: XRD patterns at 2 theta range between [44-47 °]. c: XRD patterns at 2 theta range between [30-33 °].

1(b), while the curves reveal three distinct domains for the evolution of the relative density as function of mol. % Fe_2O_3. The first domain corresponding to the range from 0 to 2, a manifest decrease in the pellets density is remarked for all considered temperature, the second domain range from 2 to 5 a manifest increase in the pellets density is remarked for all considered temperature, and the last domain range from 5 to 7, a small evolution of relative density obtained for all pellets and considered temperature.

The XRD curves of BTA+ x % mol Fe_2O_3 with x = 0, 1% and 7% for pellets sintered at 1400 °C in air for 2 hrs are shown in Fig. 3(a). For x = 0 a typical ABO_3 perovskite diffraction peaks are obtained with trace of Ba_2TiO_4 phase. Fig. 3(b) shows (for x = 0) a symmetric and large single peak around $2\theta = 45°$ [16], characterize the presence of (002) cubic peak, we can conclude that the perovskite structure is cubic. For x = 1%, Fig. 3(a) shows the coexistence of two phases BTA with perovskite structure ABO_3, and solid solution Ba $(T_{1-x}Fe_x)O_{3-d}$ with hexagonal phase confirmed by the curve in Fig. 3(c) for x = 1 shows the asymmetric peak diffract around $2\theta = 31$ °. This peak is a composite of the strongest XRD peak (101) for the cubic phase and (104) for the hexagonal phase [16], also the arbitraries intensities of peaks expected that the cubic percentage phases is more than the hexagonal phase. Fig. 3(b) (for x = 1) shows overlap between (002) peak of cubic phase and corresponded peak of hexagonal phase.

At doping level 7% mol, the Fig. 3(a) shows three phases, cubic and hexagonal phase, with small arbitraries intensities of peaks. However, unknown significant minoritary phase appears with the strongest peak around $2\theta = 56$ °.

It is noted that the XRD peaks position of Ba $(Ti_{1-x}Fe_x)O_{3-d}$ shift toward higher diffraction angle direction compared with that of a pure BTA. This issue can be visualized as an evidence for the dissolution of Fe^{3+} into the lattice structure. According to Shannon's effective ionic radii [17], Fe^{3+} with a coordination number of six has radius of 0.0645 nm, while Ti^{4+} with a coordination number of six possesses radius of 0.0605 nm [17]. It is known that the substitution site is mainly determined by ionic radius and charge, though the charge of Fe^{3+} is different from that of Ti^{4+}, the radius of Fe^{3+} is compatible with that of Ti^{4+}, so Fe^{3+} should substitute Ti^{4+} with a relatively large size. The incorporation of Fe^{3+} increased the mean radius of the B-site. This led to an increase in the dimension of the unit cells which caused the shift of XRD peaks toward lower diffraction angle direction compared with that of BTA. On the other hand, oxygen vacancies can be formed in $BaTi_{1-x}Fe_xO_{3-d}$ to maintain the overall electrical neutrality according to the Kröger-Vink equation,

$$2Fe^{3+} \xrightarrow{BaTiO_3} 2Fe'_{Ti} + V_O^{\cdot\cdot} \quad (3)$$

Table. 1. lattice parameters and tetragonality of BTR + x % mol Fe_2O_3 pellets sintered at 1400 °C.

Iron amount	Lattice parameter		Tetragonality
x%	a (Å)	C (Å)	c/a
0	3.9892	4.0198	1.0077
1	3.9453	3.9797	1.0087
7	3.9811	4.0226	1.0102

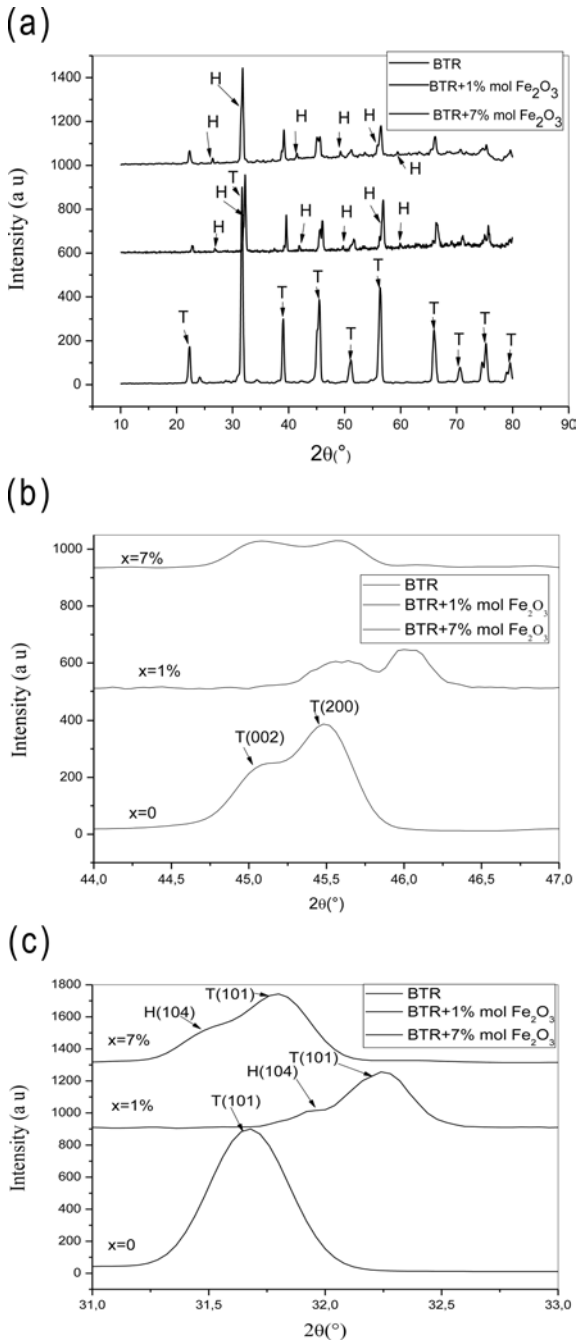

Fig. 4. a: XRD spectra recorded from BTR+ x % Fe_2O_3 samples sintered at 1400 °C for 2 hrs. T: Tetragonal, H: hexagonal. b: XRD patterns at 2 theta range between [44-47 °]. c: XRD patterns at 2 theta range between [30-33 °].

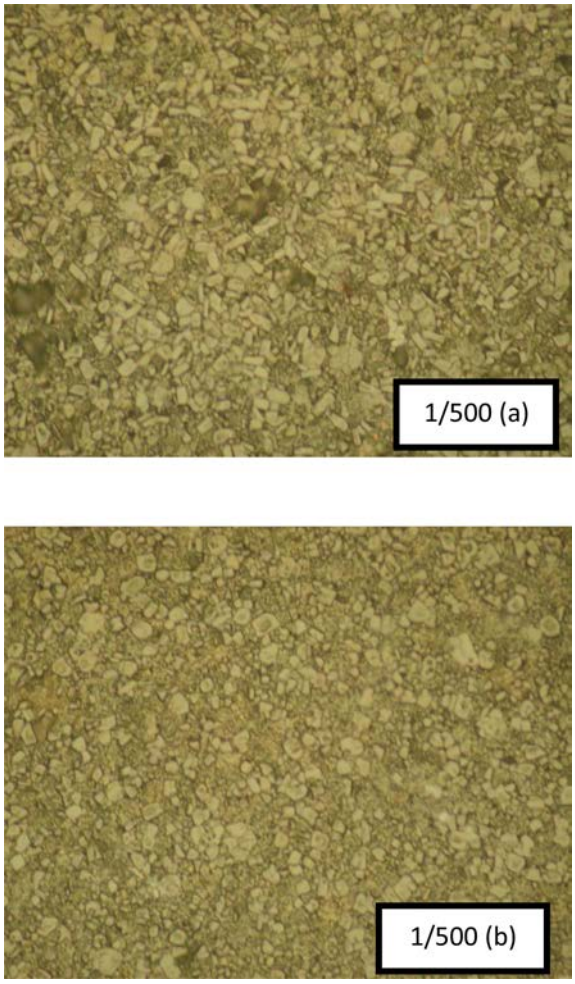

Fig. 5. Optical micrograph of pellet sintered at 1400 ºC in air for 2 hrs at 3 ºC/ min.
a- BTA + 7% mol Fe_2O_3.
b- BTR + 7% mol. Fe_2O_3.

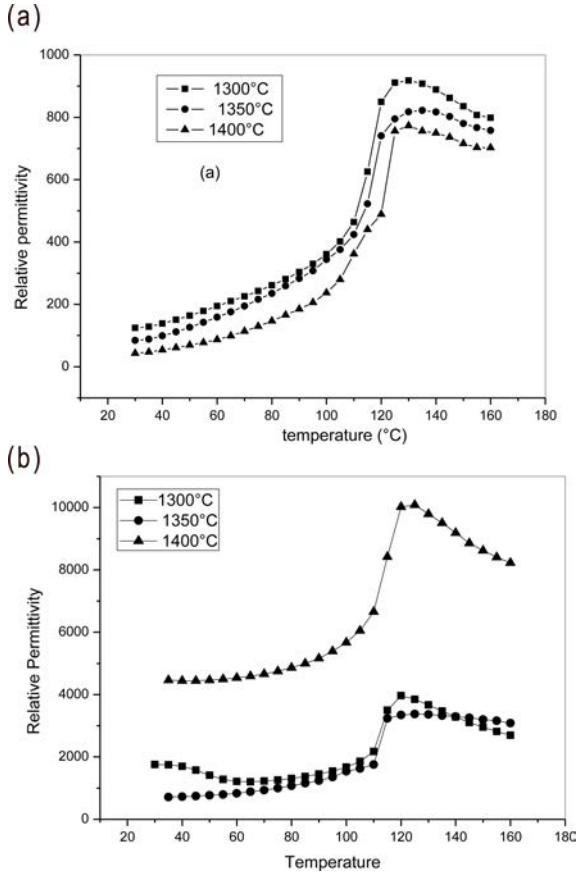

Fig. 6. Variation of the relative permittivity as function of temperature for samples sintered at 1300, 1350 and 1400 ºC
a- BT (A) + 7% mol. Fe_2O_3.
b- BT(R) + 7% mol. Fe_2O_3.

From the view point of crystal chemistry, the creation of oxygen vacancies can contribute to a decrease in the unit cell dimension, which should cause a shift of XRD peaks towards higher diffraction angle direction. The competition between the two effects is presumed to be responsible for the shift of the XRD peaks. In this case the oxygen vacancies effect was the predominant effects of Fe-doped $BaTiO_3$ ceramics. Our results agree with those obtained by other investigators on the structural and dielectrics properties of Fe-doped BT [6]. For the second mixture, XRD curves are shown in Fig. 4(a), for x = 0, a typical ABO_3 perovskite structure was obtained without detectable presence of any other phases. Similarly, the Fig .4(b) shows an asymmetric peak around $2\theta = 45$ º characterizes the presence of (002) and (200) tetragonal peaks, we conclude that the perovskite structure is tetragonal.

To confirm this result, we use the strongest peak diffract around $2\theta = 31$ º, in this respect, for x = 0 the Fig. 4(c) shows the symmetric strongest peak (101) confirmed the presence of only the tetragonal phase. For x = 1 the enlarged curve in the range [30-33 º] shows the asymmetric strongest peak composite from peaks (101) and (104), respectively, for tetragonal and hexagonal phases. These peaks shift toward higher diffraction angle direction illustrating a decrease in structure tetragonality of perovskite, also, for x = 7% the peak shows the same results, but its shifted toward lower diffraction angle direction illustrating an increase in structure tetragonality of perovskite shown in Table 1.

Furthermore, the reported curve in Fig. 4(b) confirm the noted results; for x = 1 and 7% show overlap between tetragonal peaks (200) and (002) with the corresponded hexagonal peaks, and the same observation about the peaks shift. We see that the arbitraries intensities of tetragonal peaks are stronger than those of hexagonal peaks.

The shift of XRD peaks positions for $BaTi_{1-x}Fe_xO_{3-d}$ was visualized as an evidence for the dissolution of Fe^{3+} into the lattice structure and the compensation mechanism. So the oxygen vacancies effects was predominant for the low amount of iron , while the

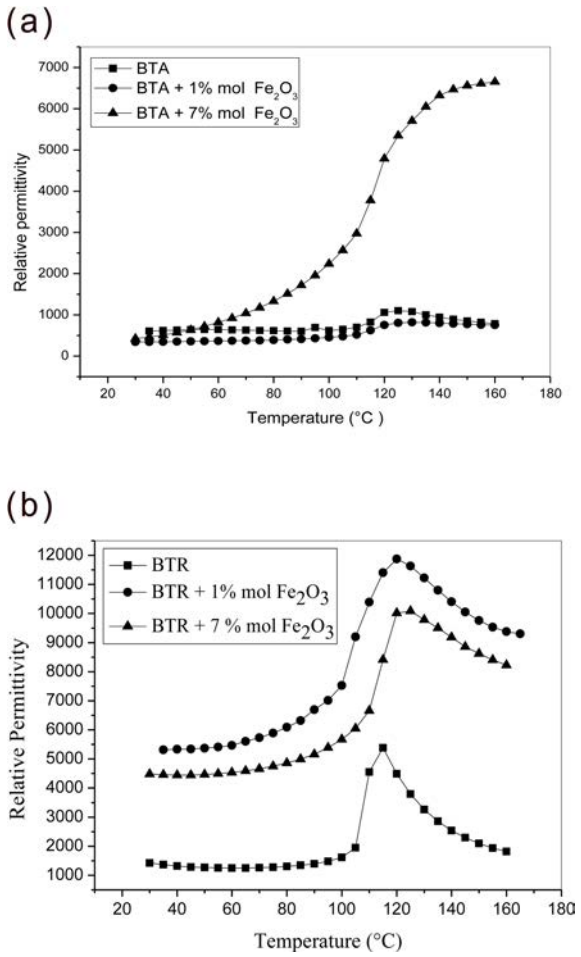

Fig. 7. Evolution of the relative permittivity as function of temperature for samples sintered at 1400 °C for 2 hrs at 3 °/min.
a- BT (A) + x %mol. Fe_2O_3.
b- BT(R) + x % mol. Fe_2O_3.

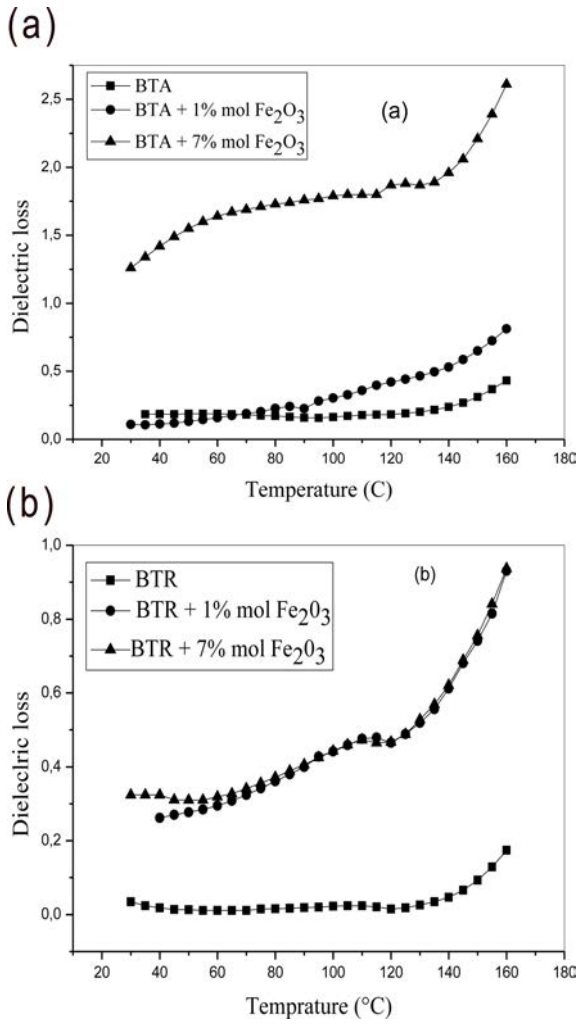

Fig. 8. Dielectric loss for samples sintered at 1400 °C. (a) – BTA+ x % mol F_2O_3 (b) – BTR+ x % mol F_2O_3

Fe^{+3} substitute Ti^{4+} in B site was the predominant effects for the large amount of Fe-doped $BaTiO_3$ ceramics.

The optical micrographic observations were shown in Fig. 5 both ceramics show dense microstructure. The Fig. 5(a) reveals the presence of 3 phases; white major phase with a great grains corresponding to BTA phase, brown phase with fine grains corresponding to hexagonal phase and dark minor phase corresponding to unknown phase. These observations agree with the results obtained by XRD analysis. Fig. 5(b) reveals the presence of 2 phases, white phase with spherical and homogeny grains corresponding to BTR phase and brown minor phase corresponding to hexagonal phase. These observations also agree with the results obtained by XRD analysis.

Concerning the influence of sintering temperature on the dielectric properties of both BTA+7% mol Fe_2O_3, and BTR + 7% mol Fe_2O_3, the Fig. 6(a) and 6(b) show the variation of the relative permittivity ε_r(T) as function of temperature for samples sintered at 1300, 1350 and 1400 °C for 2hrs. Fig. 6(a) shows the relative permittivity ε_r (T) of BTA+7% mol Fe_2O_3 for samples sintered at 1300, 1350 and 1400 °C for 2hrs.

In the opposite of the increases in the relative density of BTA+7% mol Fe_2O_3 samples sintered at 1300, 1350 and 1400 °C for 2 hrs, the reported curves reveal a decrease in the room temperature dielectric constant with increase sintering temperature. This result would be related to the parraelectric phases, cubic and hexagonal phases formed in BTA+7% mol Fe_2O_3 pellets sintered at different sintering temperatures. Also, we observe a decrease in the curie peak of transition ferro-parraelectric phase and small shift to high temperature with large diffuse. This behavior would be attributed to the incorporation of iron ions Fe^{3+} in B site of BTA lattice. Thus this result agrees with that reported in the introduction. Fig. 6(b) shows the relative constant ε_r (T) of BTR +7% mol Fe_2O_3 sintered at 1300, 1350 and 1400 °C for 2hrs, the curves

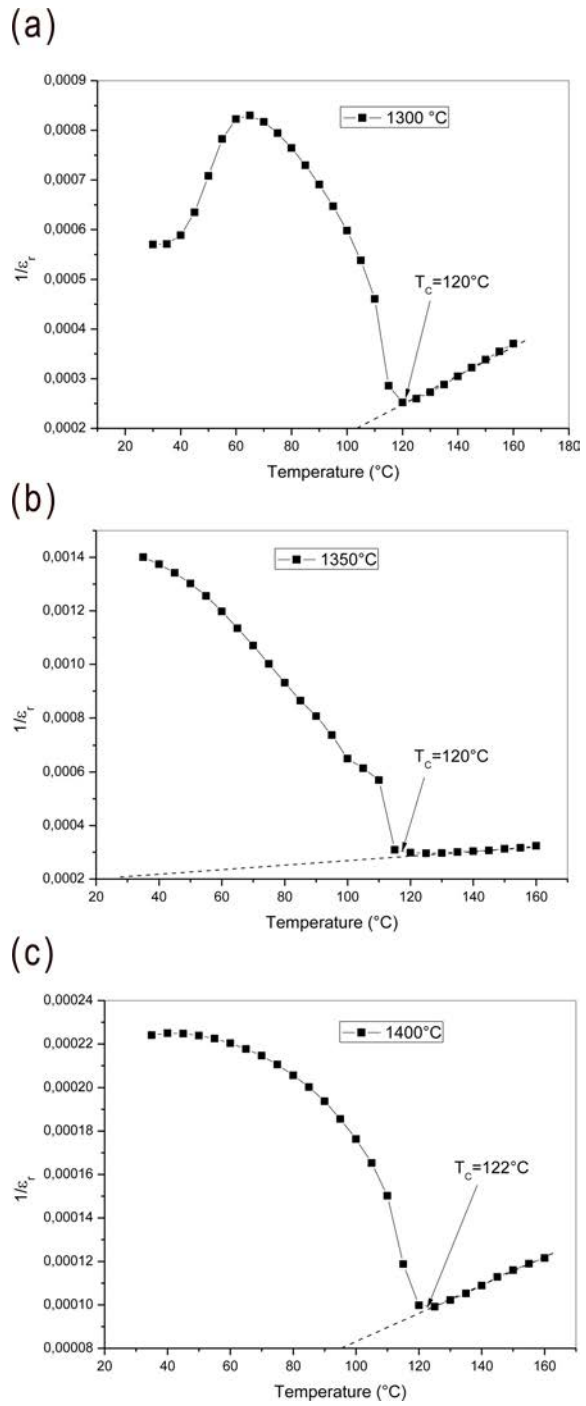

Fig. 9. Evolution of the reciprocal of dielectric constant ($1/\varepsilon_r$) at 1 KHz as function of temperature for BT(R) + 7% mol. Fe_2O_3 samples sintered at (a)1300 °C, (b)1350 °C and (c)1400 °C for 2 hrs at 3 °/ min

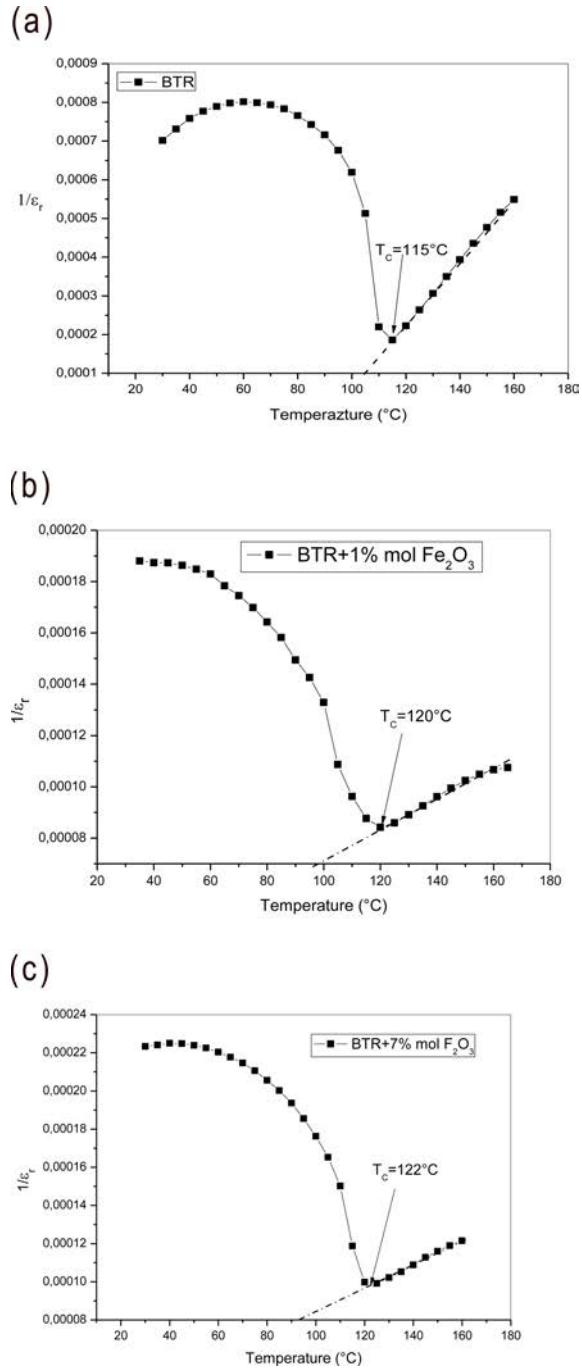

Fig. 10. Evolution of the reciprocal of dielectric constant ($1/\varepsilon_r$) at 1 KHz as function of temperature for (a)BT(R), (b) BT(R) + 1% mol. Fe_2O_3 and (c) BT(R) + 7% mol. Fe_2O_3 samples sintered at 1400 °C for 2 hrs at 3 °/ min

illustrate two evolution domains of ε_r (T). The first domain ranged between 1300-1350 °C, where ε_r (T) has the same value ~1000 at room temperature, and for the second domain ranged at 1400 °C, the reported curve reveals an obvious increase in the room temperature dielectric permittivity with sintering temperature. Here the value of ε_r varies from ~1000 in BTR+7% mol Fe_2O_3 samples sintered at 1300 and 1350 °C to ~ 4500 in BTR+7% mol Fe_2O_3 samples sintered at 1400 °C. This result would be related to two factors, (i) The increase in the relative density of BTR+7 % mol Fe_2O_3 shown above, (ii) The major ferroelectric phase formed in BTR+7% mol Fe_2O_3 pellets sintered at 1400 °C. On the other hand, we

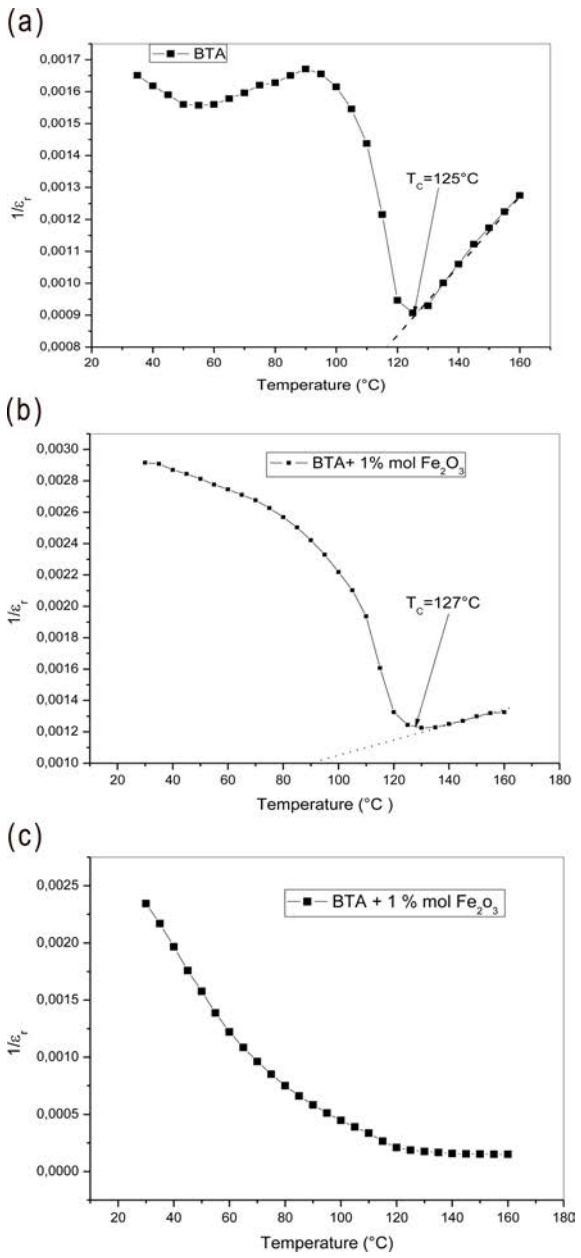

Fig. 11. Evolution of the reciprocal of dielectric constant ($1/\varepsilon_r$) at 1 KHz as function of temperature for (a)BT(A), (b) BT(A) + 1% mol. Fe2O3 and (c) BT(A) + 7% mol. Fe2O3 samples sintered at 1400 °C for 2 hrs at 3 °/ min

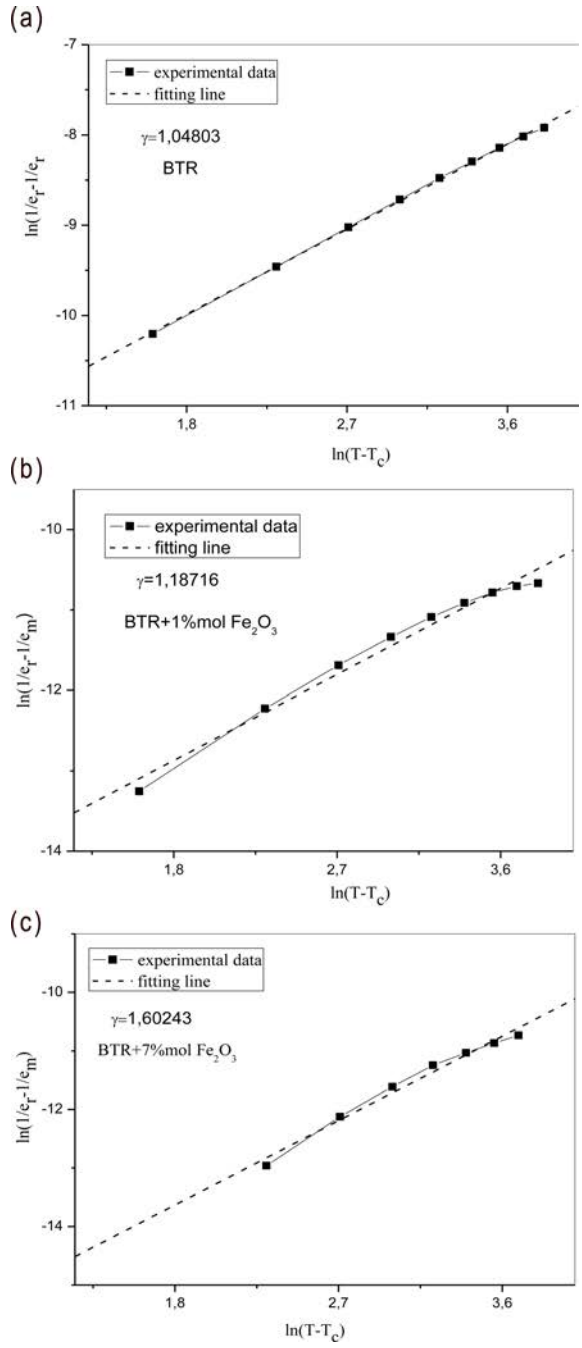

Fig. 12. Plots of ln ($1/\varepsilon_r$-1/εm) as function of ln (T-TC) at 1 KHz for BTR, BTR+1 % mol Fe2O3, and BTR+7% mol Fe_2O_3, for samples sintered at 1400 °C for 2 hrs at 3 °/min

observe that the maximum value of the relative permittivity e_m increased and shifted as a function of sintering temperature at the same time toward the high temperature. We see that e_m enhanced from ~3000 in BTR+7% mol Fe_2O_3 samples sintered at 1300 and 1350 °C to ~10000 in BTR+7% mol Fe_2O_3 samples sintered at 1400 °C, while the corresponding Curie temperature (T_C) has a small change to the high temperature, and the shift of curie peak to high temperature can be attributed to the small substitution of Ti^{4+} by iron ion Fe^{3+} in B sites. To study the effects of iron amount on dielectrics properties, we use two amounts of iron 1% and 7% mol Fe_2O_3. In the Fig. 7(a) we show the relative permittivity ε_r (T) for different Fe_2O_3 doped BTA pellets sintered at 1400 °C for 2 hrs.

The reported curves reveal the same value ~500 for different amounts of iron at room temperature. We see a small peak of curie transition appeared for the small amount of iron, and disappeared for the large amount of it. This result attributed to the parraelectric phase

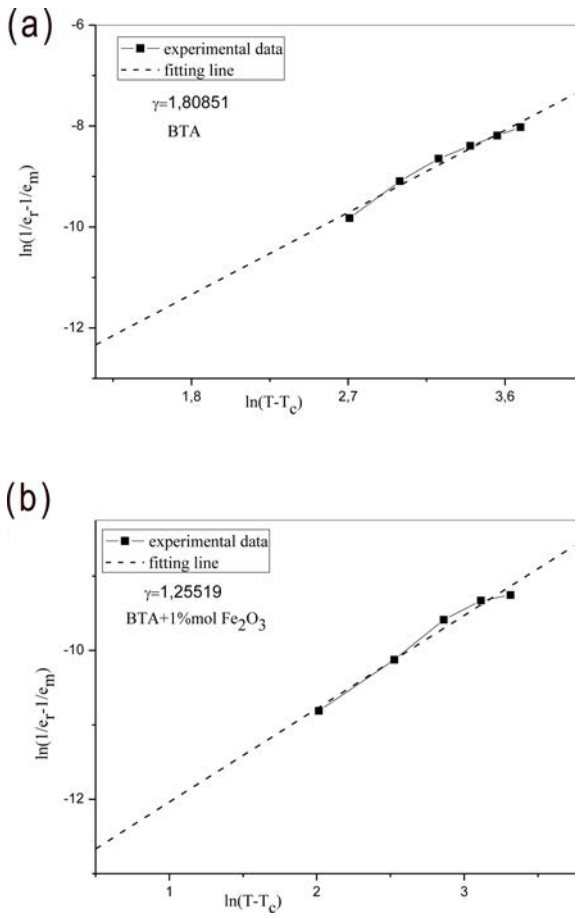

Fig. 13. Plots of ln ($1/\varepsilon_r$-$1/\varepsilon m$) as function of ln (T-TC) at 1 KHz for BTA, and BTA+1% mol Fe_2O_3, for samples sintered at 1400 °C for 2 hrs at 3 °/min

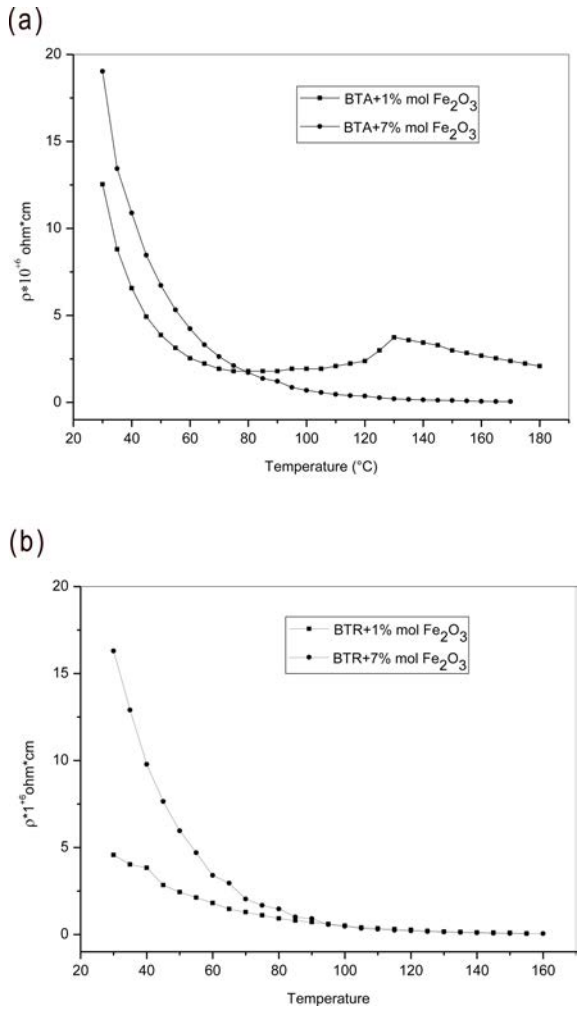

Fig. 14. Evolution of electrical resistivity ρ(T) at 100V as function of temperature for samples sintered at 1400 °C for 2 hrs at 3 °C/min (a)- BTA+ x % mol Fe_2O_3 (b)- BTR+ x % mol Fe_2O_3

formed in the pellets which reveal by XRD analysis.

Fig. 7(b) shows the relative permittivity ε_r (T) for different Fe_2O_3 doped BTR pellets sintered at 1400 °C for 2 hrs. The reported curves reveals the value ~1000 for x = 0 at room temperature, this value is higher compared with that of BTA pure, also, this value of ε_r (T) enhances for both small amount of iron (x = 1%) to ~ 5500, and for the large amount of iron (x = 7%), to ~ 4500 at room temperature. On the other hand, we see that the peak of curie transition ferro-parraelectric e_m increased and shifted as function of % mol Fe_2O_3 at the same time towards high temperature, also, ε_m enhances from ~ 5500 for small amount of iron (x = 1%) to ~ 4500 for the large amount (x = 7%), while the corresponding temperature varies from ~ 115 °C to ~ 122 °C. This result can be attributed to two factors, the oxygen vacancies for the small amount of iron and the major ferroelectric phase formed in BTR pellet contains a large amount of it. The shift of curie peak to high temperature in pellet sintered at 1400 °C can be attributed to the substitution of Ti^{4+} by Fe^{3+} in B site.

Fig. 8(a) and 8(b) show dielectric loss evolution as function of both sintering temperature and Fe_2O_3 addition in the precedent pellets. It can be seen that the room temperature dielectric loss shown in fig.8.b increases from ~ 0.05 in BTR un-doped pellets to ~0.3 in BTR doped pellet. While the loss peak corresponding to ferro-parraelectric transformation decreases with % mol F_2O_3 and its position was moved toward low temperature. Furthermore, the recorded curves of BTA+ x% mol Fe_2O_3 sintered at 1400 °C reveal a net increase in the room temperature dielectric loss from ~ 0.2 in BTA un-doped pellets to ~ 1.5 in BTA+ 7% mol Fe_2O_3 pellets. We conclude that x % mol Fe_2O_3 enhances the dielectric loss of sintered pellets, BTA+ x % mol Fe_2O_3, and BTR+ x % mol Fe_2O_3. This result attribute to the increase in the tetragonality factor caused by the phases formed in both pellets.

The ferroelectric types were studied with Curie-Weiss law [18],

$$\frac{1}{\varepsilon_r} = \frac{(T - T_C)}{C} \tag{4}$$

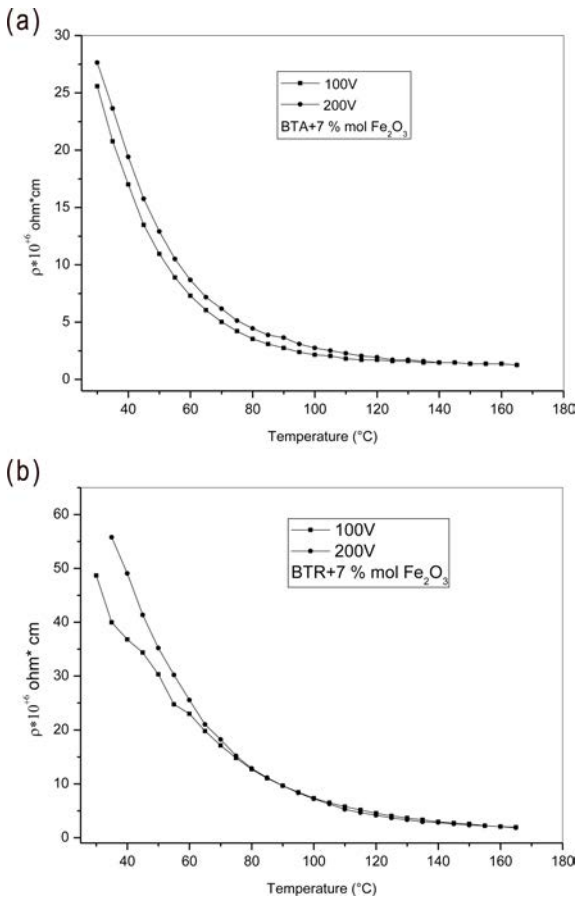

Fig. 15. effect of applied tension on the electrical resistivity as function of temperature for samples sintered at 1400 °C for 2 hrs at 3 °C/min. (a)- BTA+ 7% mol Fe_2O_3. (b)- BTR+ 7% mol Fe_2O_3

Where T_C is Curie-Weiss temperature and C is Curie-Weiss constant. The plots of $1/e_r$ at 1 KHz as function of temperature and the fitting plots by the Curie-Weiss law for BT(R) + 7% mol. Fe_2O_3 sintered at 1300, 1350 and 1400 °C for 2 hrs, respectively, are shown in Fig. 9. The data show a good linear dependence of $1/\varepsilon_r$ in term of $(T-T_C)$ in the parraelectric state above T_C for BT(R) + 7% mol. Fe_2O_3 suggesting the classical dielectric property of linear ferroelectric ceramic.

Also, Fig. 10(a, b and c) shows the reciprocal of dielectric permittivity $1/\varepsilon_r$ at 1 KHz as function of temperature and the fitting plots by the Curie-Weiss law for BT(R) + x % mol. Fe_2O_3 pellets sintered at 1400 °C for 2 hrs at 3 °/min. The reported data show also a good linear dependence of $1/e_r$ in term of $(T-T_C)$ in the parraelectric state above T_C for BT(R) + x % mol. Fe_2O_3 suggesting the classical dielectric property of linear ferroelectric ceramic.

Fig. 11(a-c) shows the reciprocal of dielectric permittivity $1/e_r$ at 1 KHz as function of temperature and the fitting plots by the Curie-Weiss law for BT(A) + x % mol. Fe_2O_3 pellets sintered at 1400 °C for 2 hrs at 3 °/ min. The reported data show a good linear dependence of $1/\varepsilon_r$ in term of $(T-T_C)$ in the parraelectric state above T_C for BT(A) and BT(A) + 1% mol. Fe_2O_3 suggesting the classical dielectric property of linear ferroelectric ceramic, this behavior disappeared for BT(A) + 7% mol. Fe_2O_3.

Then Figs. 9-11 shows a shift of Curie ferro-parraelectric phase transition to high temperature.

Han-li Lian [14] pointed out that the order of phase transition can be determined by ΔT, namely ΔT = 0 indicate the ferro-parraelectric phase transition is of a second order type, while ΔT > 0 is a first order type of phase transition, here, the ΔT values for both samples are larger than zero, suggesting a first order type phase transition.

In order to further characterize the dielectric properties, a modified Curie-Weiss law also was used [18, 19]

$$\frac{1}{\varepsilon_r}-\frac{1}{\varepsilon_m}=\frac{(T-T_C)^{\gamma}}{C'} \tag{5}$$

where ε_m is the maximum value of dielectric constant at Curie temperature Tc, C' is the Curie-Like constant and γ the degree of diffuseness. γ is usually ranging from 1 for a normal (linear) ferroelectric to 2 for an ideal relaxor ferroelectric. The plots of $ln\left(\frac{1}{\varepsilon_r}-\frac{1}{\varepsilon_m}\right)$ as function of $ln(T-T_C)$ at 1 KHz for BTR, BTR +1% mol Fe_2O_3 and BTR+7% mol Fe_2O_3 are shown in Fig. 12. All samples demonstrate a linear relationship by least-squared fitting the experimental data to the modified Curie-Weiss law, the value of γ was determined from the slope of the fitting curve.

The calculated γ for BTR is ~ 1.05 indicate a normal ferroelectric, while that for BTR+1% mol Fe_2O_3 increases to ~1.19 and for BTR+7% mol Fe_2O_3 to ~1.60. The increasing in γ value implies that there is a diffuse character in both BTR+1% mol Fe_2O_3 and BTR+7% mol Fe_2O_3. This behavior shows a partially relaxor ferroelectric for both samples which increases with the increase of iron amount. In either hand, Fig. 13 shows the plots of $ln\left(\frac{1}{\varepsilon_r}-\frac{1}{\varepsilon_m}\right)$ as function of $ln(T-T_C)$ at 1 KHz for BTA and BTA+1% mol Fe_2O_3. The calculated g for BTA is ~1.81, while that for BTR+1% mol Fe_2O_3 decreases to ~1.26 which shows a partially diffuse phase transition, such behaviour indicates a partially relaxor ferroelectric witch decreases with an increasing in iron amount in the sintered pellets, and disappeared for the big amount of iron

The diffuse phase transition behaviour refers to the coexistence of complex cations (Fe^{3+} and Ti^{4+}) at an equivalent crystallographic site. Furthermore, the formation of oxygen vacancies in the several pellets can increase the local compositional heterogeneity and therefore contributes to more diffusive characteristic of phase transition.

Fig. 14 shows the electrical resistivity ρ (T) as function of temperature [20] for both BT (A) + 7% mol. Fe_2O_3 and BT(R) + 7% mol. Fe_2O_3 samples

sintered at 1400 °C for 2 hrs at 3 °/min. The reported curves reveal a room temperature electrical resistivity which increases with the increase of the amount of iron for both samples.

Also, there is a monotonous decrease evolution of electrical resistivity as function of temperature for both samples sintered at 1400 °C for 2 hrs at 3 °/min, this evolution illustrate a semiconductor behavior [21], where Fe^{3+} ions act as an acceptor type [22].

Such behavior can be explained by the following equation in the notation of (Kröger-Vink);

$$Fe_2O_3 \rightarrow 2Fe'_{Ti} + 3O_O^X + V_O^{\cdot\cdot} \quad (6)$$

Fig. 15 shows the dependence between the electrical resistivity r(T) and applied tension as function of temperature for both BTA + 7% mol Fe_2O_3 and BTR+ 7% mol Fe_2O_3 samples sintered at 1400 °C for 2 hrs at 3 °C /min, this identical evolution which illustrates an independence between applied tension (V) and activation energy (E_g).

Conclusions

The main results of this investigation are:

1. $BaTiO_3$ ceramic was prepared via the solid state reaction method between $BaCO_3$ and both TiO_2 phases, anatase phase (A) and retile phase (R). Both ceramics show the pure perovskite structure with the cubic phase for BTA and the tetragonal phase for BTR.

2. Both Fe doped BTA and BTR ceramics with doping level of 1% and 7% molar fraction were fabricated by the same way, both cubic and hexagonal phases coexisted in the Fe doped BTA ceramics, the doping by Fe^{3+} into BTA caused a decrease in relative density compared with pure BTA, as a consequence, there is a decrease in dielectric permittivity, an increase in dielectric loss and a shift of curie peak toward high temperature.

Also both tetragonal and hexagonal phases coexisted in Fe doped BTR ceramics, the doping by Fe^{3+} into BTR caused an increase in both relative density and tetragonality, respectively, compared with pure BTR, as a consequence, we got an increase in both dielectric permittivity and dielectric loss, while the curie peaks were shifted to the higher temperature compared with the peak of the pure BTR.

3. Curie-Weiss law shows a linear ferroelectric property for Fe doped both BTA and BTR ceramics with a first order type of Curie phase transition. In other hand, the modified Curie-Weiss law shows a partially relaxor ferroelectric behavior for both Fe-doped BTA and BTR ceramics.

4. The electrical resistivity evolution in term of temperature shows a semiconductor behavior with independence between applied potential and activation energy, where Fe^{3+} ions act as an acceptor type.

References

1. D.-H. Yoon. J. Ceram. Proc. Re. 7[4] (2006) 343-354.
2. A. Graff, S. Senz, D. Voltzke, H.P. Abicht, D. Hesse, J. E. Cer. Soc. 25 (2005) 2201-2206.
3. B. Cui, P. Yu, J. Tian, Z. Chang, Mat. Sci. Eng. 133 (2006) 205-208.
4. Z. Abdelkafi, N. Abdelmoula, H. Khemakhem, R. Vonder, L. Bih, J. Allo. Comp. 427(2007) 260-266.
5. B. Cui, B. Yu, J. Tian, Z. Chang, Mater. Sci. and Eng. B133 (2006) 205-208.
6. Q. Shen-yu, L.I. Wang, L.I.U. Gui-hua, Ceram. Nonferr. Met. Soc. China 20 (2010)1911-1915.
7. G. Yqo, X.Wang, Y. Yang, J. Am. Ceram. Soc. 93 (2010) 1679-1701.
8. B.D. Stojanovic, C.R. Foscchini, M.A. Zaghete, J. Mat. Proc. Tech. 143-144 (2003) 802-806.
9. S.-H. Lee, D.-Y. Kim, M.-K. Kim, H.-K. Kim, J.H. Lee, E. Baek and J.-R. Yoon, J. Ceram. Proc. Res. 16[5] (2015) 495-498.
10. J. Kim, S.H. Yoon, Y.H. Han, J. Eu. Ceram. Soc. 27 (2007) 113-1116.
11. E. Brzozowskia, M.S. Castroa, C.R. Foschinib, B. Stojanovicb, Ceram. Inter. 28 (2002) 773-777.
12. T.A. Vanderah, W. Wang-Ng, B.H. Tobym, V.M. Browning, R.D. Shull, J. Sol. St. Chem. 143 (1999) 182-197.
13. E. Brzozowski, M.S. Castro, C.R. Foschini, B. Stojanovic, Cer. Int. 28 (2002) 773-777.
14. T.A. Vanderah, J. M. Loezos, and R.S. Roth, J. Sol. St. Chem. 121 (1996) 38-50.
15. H.-l. Lian, J. Ceram. Proc. Res. 17[7] (2016) 685-689.
16. Q. Lou, X. Shi, X. Ruan, J. Zeng, Z. Man, L. Zheng, C.H. Park, G. Li, J. Am.Ceram. Soc. 01[8](2018) 4397-4811.
17. R.D. Shannon, Acta Cristallogr. A32 (1976) 751-767.
18. J. Kim, J. Ha, J. Song, C.J. Van Tyne, H. Cho and H. Lee, J. Cerm. Proc. Res. 16[5] (2015) 619-623.
19. D.A. Tuan, L.D. Vuong, V.T. Tung, N.N. Tuan, and N.T. Duong, J. Ceram. Proc. Res. 18[12] (2017) 894-898.
20. A. Niemer, R. Pankrath, K. Betzler, M. Burianek, M. Muehlberg, World J. Cond. Matt. Phy. 2 (2012) 80-84.
21. F. T.Z. Toma, I.N. Esha, Md. Al-Amin, M.N. I. Khan and K.H. Maria, J. Ceram. Proc. Res. 18[10] (2017) 701-710.
22. Z.C. Li, B. Bergman, J. Eur. Ceram. Soc. 25 (2005) 441-445.
23. Y.H. Han, J.B. Appleby. D.M. Smyth. J. Am. Ceram. Soc. 94[2] (2010) 96-100.